Majlesi Journal of Electrical Engineering
Vol. 18, No. 1, March 2024

Simultaneous Optimization of Optical Characteristics of Square-Shaped Benzene-Core Photonic Crystal Fiber Based on Non-uniform Air Holes

Bao Tran Le Tran[1], Lanh Chu Van[1]
1- Department of Physics, Vinh University, Vinh, Vietnam.
Email: letranbaotran212@gmail.com, chuvanlanh@vinhuni.edu.vn (Corresponding author)

ABSTRACT:
In this paper, benzene-core photonic crystal fibers (B-PCFs) with non-uniform air holes for the square lattice are studied by controlling the air-filling factor of the air holes in the first ring and increasing those up to a maximum for external holes. Commercial Mode Solutions software is used to study the influence of structural parameters on the nonlinear coefficient, dispersion, effective mode area, and attenuation. It can be seen that this design affects the linear and nonlinear properties at the same time. In other words, it has a crucial effect on either the near-zero flatness of dispersion or going up the nonlinearity and falling the loss of the B-PCFs. The above benefits make the optimized fibers suitable for supercontinuum (SC) generation applications.

KEYWORDS: Benzene-Core Photonic Crystal Fiber; Nonlinearity; Hollow-Core; Square Lattice; Dispersion.

1. INTRODUCTION

For applications in optical technology, controlling chromatic dispersion in optical fibers becomes a crucial requirement. For instance, optical frequency measurement systems and photonic feeds are reconfigurable through wavelength tuning in the dispersive fiber and based on dispersive delay differences [1], [2]. In particular, for ultra-short pulse transmission for broadband supercontinuum (SC) generation, the behavior of ultra-flattened dispersion fibers is a goal that scientists always aim for [3], [4].

A photonic crystal fiber (PCF) with solid-core, i.e. a fiber consisting of a defect surrounded by cyclically arranged air holes, has been of great interest because of its excellent ability to control chromatic dispersion and nonlinearity through varying structural parameters, Fig. 1a. Several exciting studies of dispersion characteristics have been carried out in solid-core fibers for various applications, including wavelength shift zero dispersion (ZDW), all-normal flat dispersion, and optimized chromatic dispersion [5]-[9]. Solid PCFs can be made of different types of glass [8]-[14]. The silica glass PCFs are proven to be effectively used to generate coherent SC in the visible-to-near-infrared region. Meanwhile, non-silica fibers such as chalcogenide, tellurite, and fluoride glasses allow SC to preserve pulses in the mid-infrared. However, the SC broadening inside the silica fibers is limited because of the low nonlinear silica and large absorption in the mid-infrared region [13], [14]. On the other hand, soft glass fibers have steep dispersion in the near-infrared and often require a complex pumping system. Their toxicity is also a concern in practical applications, such as biomedical applications [15].

Paper type: Research paper
https://doi.org/10.30486/mjee.2024.2000133.1307
Received: 15 October 2023; revised: 29 November 2023; accepted: 3 January 2024; published: 1 March 2024
How to cite this paper: B. T. Le Tran, and L. Ch. Van, **"Simultaneous Optimization of Optical Characteristics of Square-Shaped Benzene-Core Photonic Crystal Fiber Based on Non-uniform Air Holes"**, *Majlesi Journal of Electrical Engineering*, Vol. 18, No. 1, pp. 241-251, 2024.

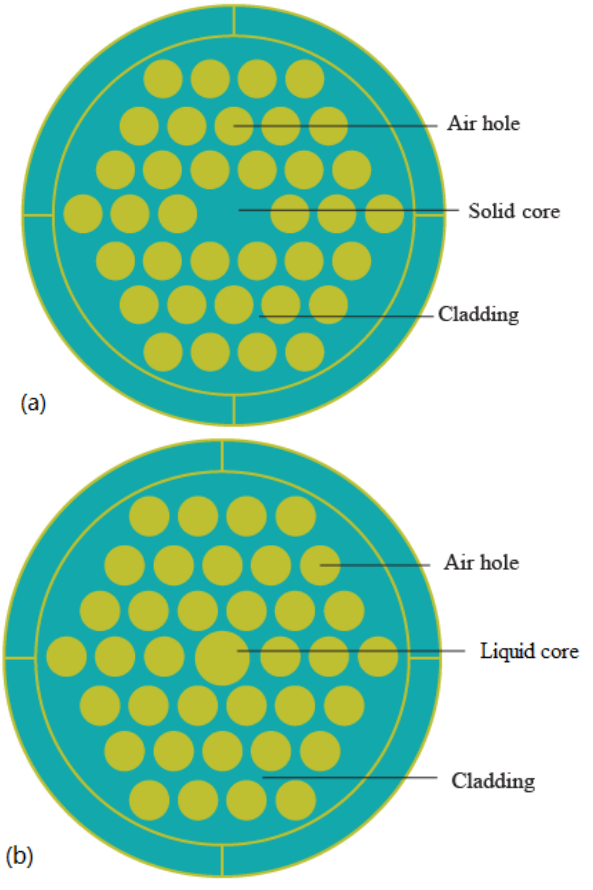

Fig. 1. Cross section of PCFs: (a) solid core and (b) liquid core.

The high nonlinear refractive index is also a factor closely related to SC generation [13]. Therefore, the use of highly nonlinear liquid-core PCFs as an excellent alternative has been considered in recent years (Fig. 1b). In practice, this approach requires a liquid reservoir to maintain the fluid in the fiber core, and the fluid tends to leak out of the cladding when infiltrated into the core. Even so, these can be remedied by modern methods such as UV-adhesive or laser writing techniques [16], [17]. Therefore, liquid core PCF can take full advantage of all the outstanding benefits of high transparency, high nonlinearity, and large photothermal coefficient of the liquid to optimize fiber properties. For example, carbon disulfide has a nonlinear refractive index 100 times higher than fused silica but its high toxicity is the problem [15]. Chloroform has low toxicity with a nonlinear refractive index lower than that of fused silica [18]. The toxicity of carbon tetrachloride is also moderate and its transparency is high in the near-infrared range. Nevertheless, the disadvantage of this liquid is that the nonlinear coefficient is not high since the linear refractive index of silica is similar to that of carbon tetrachloride [13]. Benzene is a better choice due to its nonlinear refractive index higher than some commonly used liquids such as carbon tetrachloride, tetrachlorethylene, and chloroform. This value is similar to nitrobenzene and toluene and is 61 times higher than fused silica [19]-[21]. Furthermore, there is no need to worry about attenuation of some parts of the spectrum in the wide wavelength range (0.5-1.4 μm) because benzene is less absorbed in this region. The popularity of this material has been proven when it is present in the production processes of crude oil, plastics, gasoline, etc [19]. A large number of works focusing on studying the characteristics of benzene core PCF and applying these results to SC generation have been carried out in recent years [19], [22]-[24]. Islam et al. [23] introduced a new benzene core PCF based on a plasma sensor with a high digital aperture, high sensitivity, and low loss in the 0.7-1.9 μm wavelength range. An SC wider than two octaves is generated in a benzene-core PCF with 2 nJ input energy [19]. To the best of our knowledge, it is quite difficult to simultaneously control the characteristic quantities in PCFs with the same air-hole diameter in the cladding. Recently, a novel design with differences in the size and spacing of air holes in circular benzene-PCFs was investigated by Duc et al. [24]. Although achieving ultra-flat, near-zero dispersion along with high nonlinearity and low loss is suitable for SC generation application, this structure is expected to face many difficulties in fiber production in experiments.

In the present study, we propose a benzene-core PCF (B-PCF), in which the air-filling factor in the first ring is

varied in the range of 0.3-0.8 while the figure for the other rings remains unchanged. The main purpose of this modification is to control the dispersion and other optical properties of the fiber simultaneously. Indeed, after the successful completion of all numerical studies, the proposed B-PCFs assure high nonlinearity, low loss, and near-zero flat dispersion curves over a wider wavelength range than some current designs. Here, we do not use a common lattice such as a regular hexagonal lattice but construct the air holes in the cladding into a square one. This is due to the roles of this type of lattice in applications of dispersion compensation, high birefringence, reducing propagation loss, and high nonlinearity for SC generation light source design [5], [25].

2. LINEAR PARAMETERS OF MATERIALS

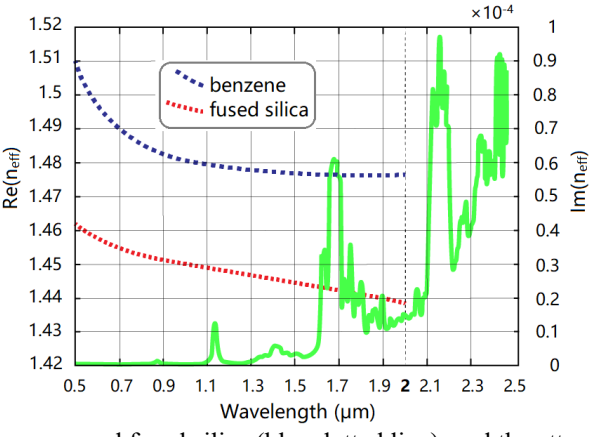

Fig. 2. The refractive index of benzene and fused silica (blue dotted line), and the attenuation characteristic of benzene (red dotted line).

It is known that the basic hollow-core PCF requires the refractive index of the core to be smaller than that of cladding so that the light propagates in the PCF according to the photonic band gap mechanism [26]. Here, we assume fused silica as a background material whose refractive index (blue line) is always less than that of benzene (red line) at whole wavelengths, Fig. 2. Therefore, like the solid core PCF, the guided modes in B-PCF obey the phenomenon of total internal reflection. The linear real part of fused silica (n_1) and benzene (n_2) is given by the Sellmeier equation and the Cauchy equation as follows [22], [27], [28]

$$n_1 = \sqrt{1 + \frac{a_1\lambda^2}{\lambda^2 - b_1} + \frac{a_2\lambda^2}{\lambda^2 - b_2} + \frac{a_3\lambda^2}{\lambda^2 - b_3}} \quad (1)$$

$$n_2 = \sqrt{c_1 + c_2\lambda^2 + \frac{c_3}{\lambda^2} + \frac{c_4}{\lambda^4} + \frac{c_5}{\lambda^6}} \quad (2)$$

where a_1 = 0.6694226, a_2 = 0.4345839, and a_3 = 0.8716947.

b_1 = 0.0044801 μm^2, b_2 = 0.013285 μm^2, and b_3 = 95.341482 μm^2.

c_1 = 2.170184597, c_2 = 0.000593990 μm^2, c_3 = 0.023034640 μm^2, c_4 = -0.000499485 μm^4, and c_5 = 0.000178796 μm^6.

The attenuation characteristic of benzene in the spectral range from 0.5 to 2.5 μm is performed using a sample in a 10 nm standard cuvette. In this setup, a halogen lamp acts as the illumination source, and two spectrometers Ocean NIR-QUEST and Thorlabs CCS200 serve as spectral analyzers in the visible and near-infrared range [22]. As observed in Fig. 2, the selected liquid has three main absorption peaks around 1.66 μm, 2.15 μm, and 2.4 μm. Meanwhile, it has high transparency in the wavelength range of less than 1.6 μm.

3. PROCESS FOR DESIGN AND SIMULATION OF B-PCF STRUCTURES

Commercial software Lumerical Mode Solutions (LMS) is used to design a B-PCF structure with a square lattice [29]. The process is described in three main steps. First, the linear parameters of the material are entered into the LMS database. Next, the fused silica base material is created in the structures. The original geometry of B-PCF consisted of eight circular air hole rings with diameter d arranged in a square lattice surrounding a central hole of the same diameter that served as the core. In the 2nd stage, we adjust the diameter of the innermost air holes d_1 such that the

filling factor $f_1 = d_1/\Lambda$ varied in the range 0.3-0.8 to control the dispersion curve, where Λ is the distance of two consecutive air holes. To optimize the loss characteristics simultaneously, the air holes in the subsequent rounds are enlarged to the diameter $d_2 = 0.95\Lambda$ [30]. The core is then infiltrated with benzene with a reasonable core diameter of $D_C = 2\Lambda - 1.1d_1$ which ensures the technical feasibility of the manufacturing process. After achieving the desired structure, the scattering boundary conditions added to the outside of the Anisotropic Perfectly Matched Layer are used to absorb without reflecting the electromagnetic wave [31]. In other words, a Perfectly Matched Layer is defined as a rectangular frame surrounding the fiber structure as shown in Fig. 3.

B-PCF can be realized by the stack-and-draw method with the individual tubes created first [32]. Then, they are stacked according to the design sample, i.e. square, in a round glass tube. The initial preform is created to be a few millimeters in size before being drawn and forming a protective jacket for the B-PCF in the fiber tower. What comes next is filling the fiber core with C_6H_6 based on a microfluidic system [13]. Fusion splicer [33] or UV-adhesive techniques [16] demonstrate their role in the proposed fibers splicing with standard single-mode ones.

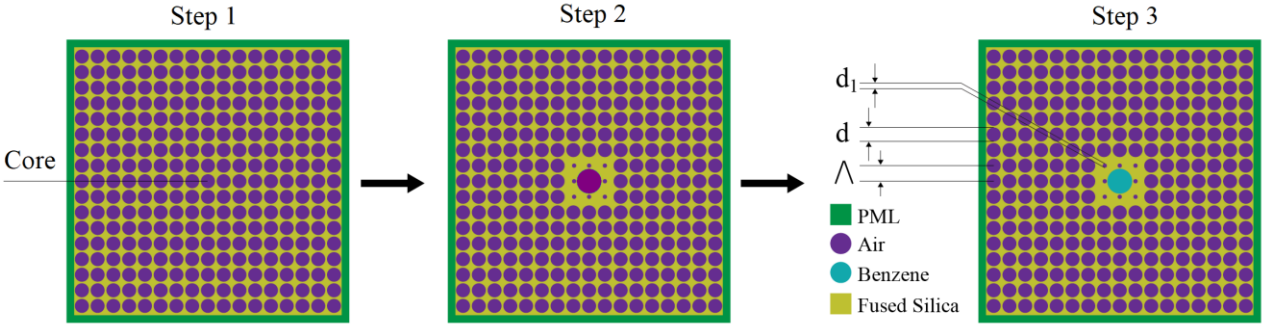

Fig. 3. Process for design of B-PCF structures.

The optical properties of the fundamental mode are calculated using the Full-vector Finite-Difference method with the mesh size smoothed to divide the solution domain into mesh elements according to the size of the fiber to increase the exact. According to Zhu and Brown [34], the Finite-Difference Eigenmode solver computes the spatial configuration by solving Maxwell's equations on a waveguide cross-sectional grid. A matrix eigenvalue problem is constructed and then solved using sparse matrix techniques to reach the mode configuration and efficiency index of the waveguide modes. Fig. 4 is a typical example of a z-normal eigenmode solver simulation with vector fields $E(x,y)e^{(-\omega t+\beta z)i}$ and $H(x,y)e^{(-\omega t+\beta z)i}$. The effective refractive index is determined

$$n_{eff} = \frac{\beta c}{\omega} \quad (3)$$

where β is the propagation constant and ω is the angular frequency.

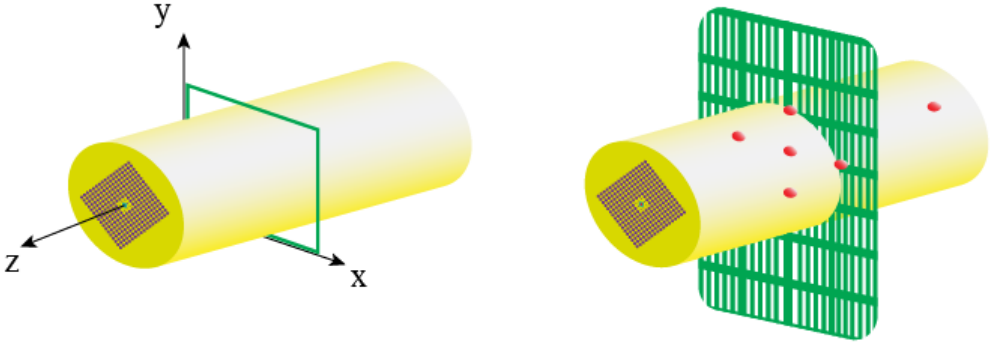

Fig. 4. A z-normal eigenmode solver simulation using the Full-vector Finite-Difference method.

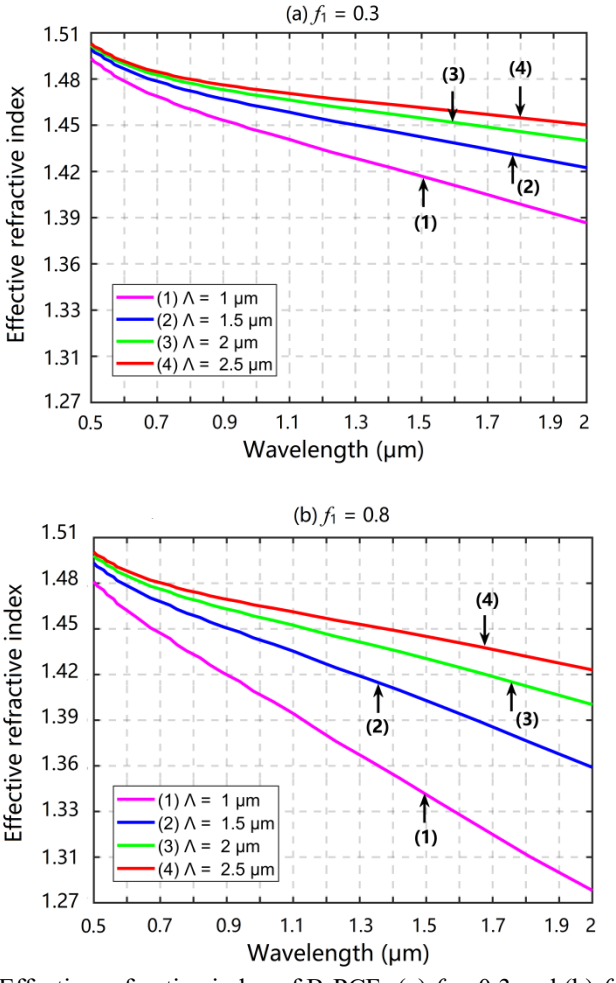

Fig. 5. Effective refractive index of B-PCFs (a) f_1 = 0.3 and (b) f_1 = 0.8.

To orient the optimal structure for SC generation, we investigate a series of simulations with pitch fluctuations Λ taking into account the limitations of commonly used methods for PCF fabrication. The empirical formula based on finite element programs offers limits of parameters in the range $0.2 < d/\Lambda < 0.8$. Assuming this value is equal to 0.1, the weak influences of waveguide dispersion cannot compensate for material dispersion at short wavelength areas. With the goal of meeting the transmission performance, we consider fibers with pitch Λ from 1.0 to 2.5 μm and filling factor f_1 varying from 0.3 to 0.8. An increase in pitch and filling factor leads to an increase in the air hole size. This means a reduction in the core diameter. In Fig. 5, we describe the effective refractive index as a function of wavelength in the case of maximum and minimum f_1. Fibers with low filling factor f_1 = 0.3 have higher n_{eff} values and their curves have a lower slope than f_1 = 0.8. This is due to the lesser contribution of fused silica in the cladding index and the expansion of the benzene core. The interaction between light and the nonlinear medium becomes stronger in small core B-PCFs, causing large slopes in the effective refractive index curves.

Chromatic dispersion (D) is an important parameter in short pulse propagation with different phase velocities and their nonlinear interactions in optical fibers (4). Optimizing this feature will find good candidates for SC generation to be suitable [35]. The previous scheme to adjust an ultra-flattened dispersion profile can be easily formulated in terms of optimization algorithms such as particle swarm optimization [36] and genetic algorithms [37]. The fact is that the use of these optimizations can lead to structures with better optical properties but are much more time-consuming to simulate. The influence of the change of the pitch and filling factor on the chromatic dispersion characteristic has been studied and shown in Fig. 6.

$$D = -\frac{\lambda}{c}\frac{d^2}{d\lambda^2}\mathrm{Re}\left(n_{eff}\right) \qquad (4)$$

where c represents the light velocity in free space and Re(n_{eff}) is the real part of the effective refractive index [12].

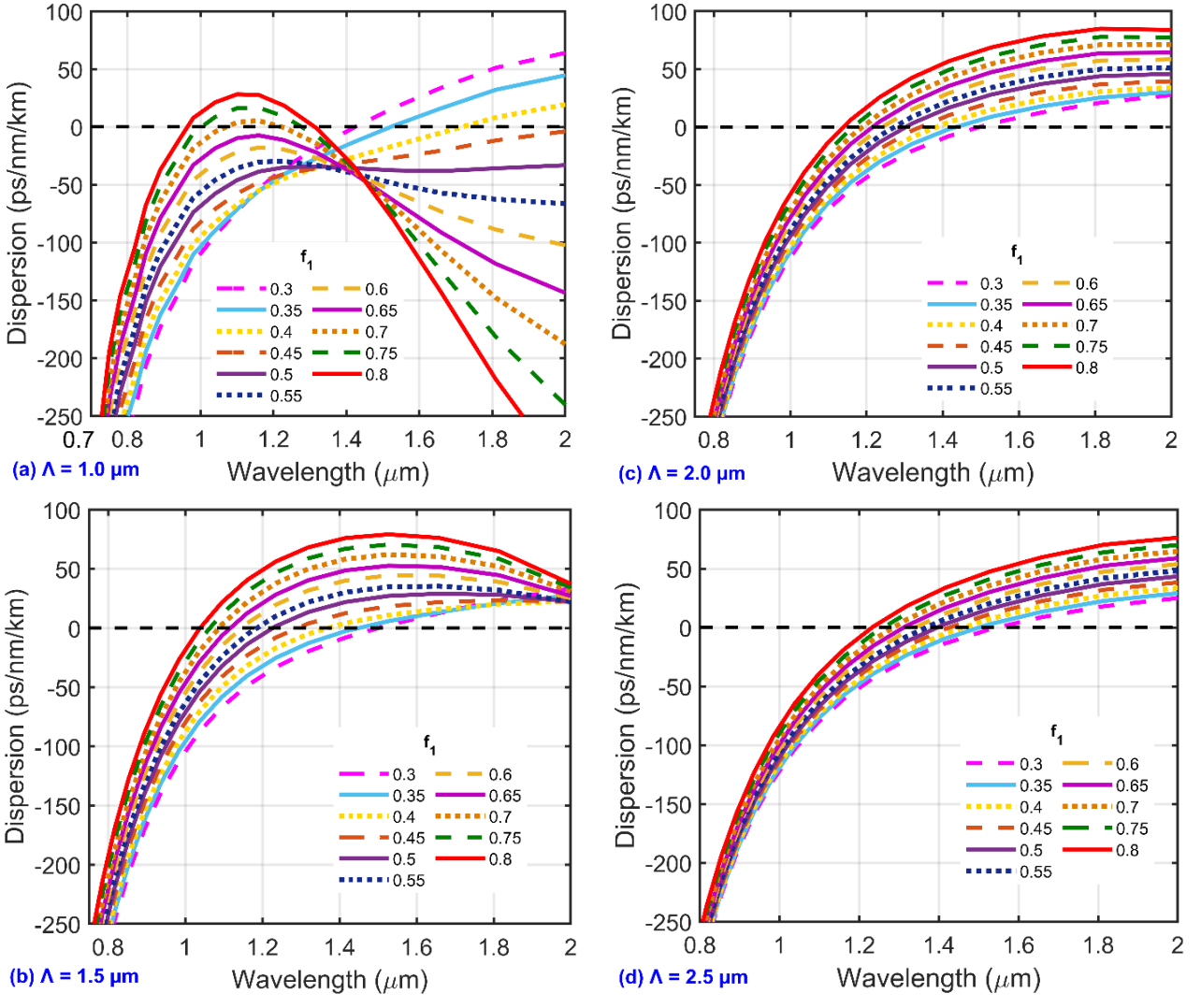

Fig. 6. Chromatic dispersion curves of B-PCFs with f_1 = 0.3-0.8 and Λ = 1.0-2.5 μm.

The key factor to achieving wide nearly zero flattened dispersion characteristic is that the slope of the linear part of dispersion curves must be forcefully controlled. In this aspect, the real part of the effective refractive index curves becomes crucial. In the case of f_1 = 0.3, the fiber with the highest pitch size is expected to be an excellent factor for SC generation since the flat profile of Re(n_{eff}) aids in flattening the dispersion curve. The figures indicate the same behavior of chromatic dispersion for the large core B-PCFs ($\Lambda \geq 1.5$ μm). The increase in the filling factor draws ZDWs to a smaller value by a small amount, and its reduction lowers the dispersion at larger wavelengths. In the short wavelength range, light scattering processes take place to a greater extent, thus the dispersion curves have huge slopes. Although displaced, the linear portion of these curves remains nearly constant in slope when the pitch is changed. This property will be very helpful in the design process. With the smallest pitch (Fig. 6a), we can achieve negative and positive dispersion profiles with one and two points of contact with zero dispersion due to the influence of waveguide dispersion [18].

The variation of structural parameters of B-PCFs such as pitch and filling factor is very small, e.g. 0.5 for the former and 0.05 for the latter. This leads to a good agreement with the error in the fiber fabrication process by the stack-and-drawn method (around 50 nm) [32]. Therefore, flattened profiles of dispersion described in Fig. 6 can be exploited to obtain desired structures without relying on complex optimization algorithms. The three negative, near-zero, and positive dispersion fibers are shown in Fig. 7 with the potential for wide spectrum bandwidth focusing on the latter, i.e. anomalous dispersion fiber. Meanwhile, the smooth and highly coherent characteristics of the spectrum depend on all-normal dispersion (negative dispersion). All-normal dispersion in Fig. 6a shows that fiber with f_1 = 0.5

behaves more smoothly in the 1.2-2 μm wavelength region. On the other hand, we need the D curve to be closer to the zero dispersion at the survey wavelength zone such as B-PCF with $f_1 = 0.65$. A similar argument, but with two ZDWs, can be used to show why the filling factor of 0.75 is chosen as the optimal one. Besides, according to Fig. 6d, the flatness and near-zero of $f_1 = 0.3$ are still superior even when all the large core B-PCFs show the same properties. This is completely consistent with the prediction in Fig. 5a.

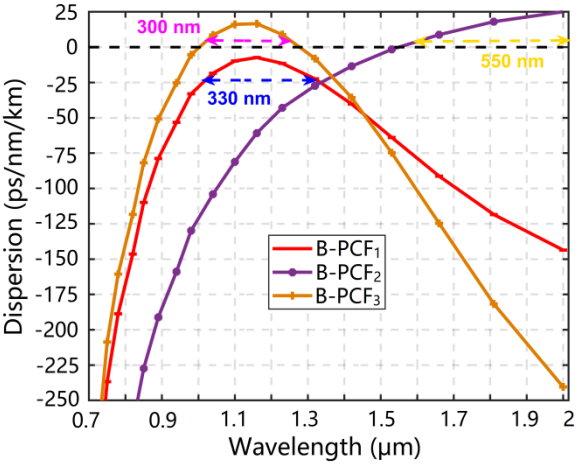

Fig. 7. Dispersion characteristics and flat dispersion range of the proposed B-PCFs.

Table **Error! Bookmark not defined.**. The parameters of the optimized B-PCFs and their flattened chromatic dispersion profiles of the proposed fibers compared with previous publications.

Ref.	The number of ZDW	f	Λ (μm)	Flat D range (nm)
B-PCF$_1$	-	0.65	1.0	330
B-PCF$_2$	One ZDW	0.3	2.5	550
B-PCF$_3$	Two ZDWs	0.75	1.0	300
[18]	-	0.65	1.0	270
[18]	One ZDW	0.3	2.0	310
[18]	Two ZDWs	0.7	1.0	225
[19]	One ZDW	0.6	2.5	145
[20]	One ZDW	0.45	4.0	520
[24]	One ZDW	0.3	2.0	290
[38]	-	0.6	1.0	250
[38]	One ZDW	0.3	2.0	400
[39]	Two ZDWs	0.8	1.0	290
[40]	-	0.6	2.0	350
[40]	One ZDW	0.6	2.0	400
[41]	One ZDW	0.9	2.2	400

In Table 1, we present the structural parameters and symbols of the optimized fibers and highlight their advantage of a flat dispersion over a wide wavelength range compared to some previous liquid-core works. Apparently, our proposed fibers are superior thanks to a wider flat dispersion range, especially B-PCF$_2$. Notably, it is possible to control further the dispersion curve by selectively filling the air holes with organic optofluidics. Indeed, the work [40] obtained a flat all-normal dispersion range equivalent to the B-PCF$_1$ when assuming that the first three inner rings are infiltrated with an optofluidic of index $n_f = 1.3$. However, the restriction appears in the anomalous dispersion region with $n_f = 1.32$ and 1.38. A more advanced configuration with a core made of C_7H_8 and the cladding material consisting of CCl_4, $CHCl_3$, allows near-zero dispersion in the 1.6-2 μm wavelength range, narrower than 500 nm of B-PCF$_2$ [41].

Subsequently, the attenuation of three structures is analyzed as seen in Fig. 8. The attenuation of B-PCF$_2$ is greatest while the shape of B-PCF$_1$ is almost the same as that of B-PCF$_3$. In particular, we find the attenuation peaks at wavelength 1.66 μm, which completely coincide with the absorption peak of benzene in Fig. 2. There is no doubt that the attenuation here is dominated by the loss material of the liquid used. This means that confinement loss is neglected

since the nonlinear refractive index of benzene ($n_2 = 16.8\times10^{-19}$ m^2 W^{-1} at 1.064 μm) is much larger than that of silica. In fact, a gap in the SC spectrum tends to arise at this attenuation peak. Even so, the high nonlinear refractive index of benzene again allows to reduce its influence when SC is generated in a short fiber sample on the order of a few centimeters [19]. Nonlinear coefficient and effective area are other important parameters for SC generation. The nonlinearity (solid lines) and effective area (dotted lines) variation for the optimized B-PCFs have been presented in Fig. 9 for the entire band of wavelength. These two quantities are related to each other through the following formula:

$$\gamma = \frac{2n_2\pi}{A_{eff}\lambda_p} \quad (5)$$

Where γ is the nonlinear coefficient, A_{eff} is the effective mode area, and λ_{p} is the pump wavelength. For the three selected fibers, λ_{p} is 1.3, 1.55, and 1.2 μm for B-PCF$_1$, B-PCF$_2$, and B-PCF$_3$, respectively. This value is chosen on the basis of being near and greater than the point of maximum dispersion and the ZDW. Since the nonlinear coefficient is inversely proportional to the effective mode area, and hence their configurations are contradictory. There is a clear separation in γ and A_{eff} curves of B-PCF$_2$ compared to small core B-PCFs. At 1.55 μm, the γ value of B-PCF$_2$ is about 860 (W.km)$^{-1}$, lower than 5390 and 6721 (W.km)$^{-1}$ of B-PCF$_1$ and B-PCF$_3$, respectively because of its larger effective mode area. In general, such nonlinearity is 10 times higher than that of [38] and even 21 times higher than [20]. Moreover, the attenuation for all three fibers is lower than that of some previous publications [42], [43]. Their values are 0.38, 3.48, and 0.54 dB cm^{-1}, respectively. The relatively high loss and small nonlinearity of previous studies may be due to the uniformity in the fiber structure and small n_2. It is clear that our design can simultaneously control the characteristics of B-PCF, making near-zero flat dispersion, low loss, and large nonlinearity suitable for SC generation. In particular, the all-normal dispersion fiber B-PCF$_1$ which can produce smooth and highly coherent SC has great potential in low-noise amplifiers and multibeam pump-probe technique [44], [45]. By contrast, the broadband SC spectrum in the remaining two structures supports various types of sensors or biomedical applications [46], [47].

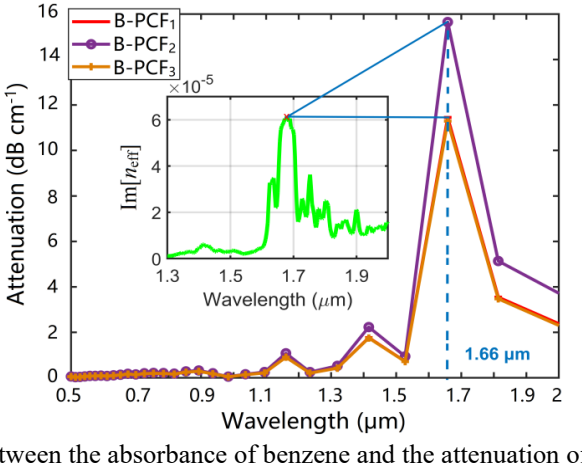

Fig. 8. The suitability between the absorbance of benzene and the attenuation of the suggested B-PCFs.

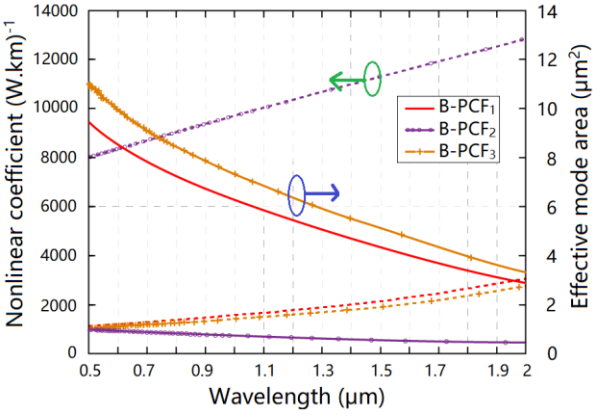

Fig. 9. The nonlinearity (solid lines) and effective area (dotted lines) of the optimized B-PCFs.

4. CONCLUSION

The influence of the change in the air hole size on the nonlinearity, dispersion, attenuation, and effective mode area for benzene-filled hollow-core PCFs with square lattice has been investigated. As for the simulation of dispersion characteristics of the structures, fibers with flattened near-zero all-normal dispersion (B-PCF_1) and dispersion with one or two ZDWs (B-PCF_2 and B-PCF_3) were selected as the optimal structures for SC generation. Since the nonlinear coefficient is inversely proportional to the effective mode area for a given wavelength, this means that the small A_{eff} of B-PCF_1 and B-PCF_3 increases their γ values with respect to that of B-PCF_2. The attenuation for the three types of B-PCFs is negligible at the pump wavelength used and reflects the correlation between material loss and fiber attenuation. Generally speaking, the size difference of the air holes simultaneously affects the optical characteristics, and hence the attenuation and effective mode drop significantly, while it also has an important impact on the dispersion and on the nonlinearity.

Data Availability. Data underlying the results presented in this paper are available from the corresponding author upon reasonable request.

Funding. Le Tran Bao Tran was funded by the Master, PhD Scholarship Programme of Vingroup Innovation Foundation (VINIF), code VINIF.2023.TS.133.

Conflicts of interest. The authors declare no conflict of interest.

Ethics. The authors declare that the present research work has fulfilled all relevant ethical guidelines required by COPE.

REFERENCES

[1] H. Emami, M. Ashourian, and M. Ebnali Heidari, **"Dynamically Reconfigurable All Optical Frequency Measurement System,"** *J. Lightwave Tech.*, vol. 32, pp. 4194-4200, Dec. 2014.

[2] H. Emami, N. Sarkhosh, E. R. L. Lara, and A. Mitchell, **"Reconfigurable Photonic Feed for Sinuous Antenna,"** *J. Lightwave Tech.*, vol. 30, pp. 2725-2732, Aug. 2012.

[3] A. Al-Kadry, L. Li, M. E. Amraoui, T. North, Y. Messaddeq, and Ma. Rochette, **"Broadband supercontinuum generation in all-normal dispersion chalcogenide microwires,"** *Opt. Lett*., vol. 40, pp. 4687-4690, Oct. 2015.

[4] C. V. Bien, L. V. Hieu, H. V. Chin, N. T. Thao, H. V. Thuy, H. D. Quang, and C. L. Van, **"Silica-based Photonic Crystal Fiber for Supercontinuum Generation in the Anomalous Dispersion Region: Measurement and Simulation,"** *Communications in Phys*., vol. 32, pp. 369-377, Aug. 2022.

[5] L. T. B. Tran, D. V. Trong, C. V. Lanh, N. T. H. Trang, H. T. Duc, and N. T. Thuy, **"Nonlinear properties of circular solid-core photonic crystal fiber with the difference of air-hole diameters and the spacing of air-holes in the cladding,"** *Hue Univ. J. Sci. Natural Sci*., vol. 131, pp. 13-21, Dec. 2022.

[6] S. J. Raja, T. Jose, R. Charlcedony, M. S. Paul, and R. Chakravarthi, **"Design of hexagonal chalcogenide photonic crystal fiber with ultra-flattened dispersion in mid-infrared wavelength spectrum,"** *Beni-Suef Univ. J. Basic Appl. Sci*., vol. 11, 103 (9pp), Aug. 2022.

[7] E. K. Akowuah, P. A. Agbemabiese, and A. K. Amoah, **"Ultra-high birefringence with tuneable double zero chromatic dispersion-PCF: a theoretical analysis,"** *J. Electrical Systems and Inf. Technol*., vol. 10, 25 (20pp), Apr. 2023.

[8] H. Saghaei, **"Dispersion-engineered microstructured optical fiber for mid-infrared supercontinuum generation,"** *Appl. Opt*., vol. 57, pp. 5591-5598, Jul. 2018.

[9] H. Saghaei and V. Van, **"Broadband mid-infrared supercontinuum generation in dispersion-engineered silicon-on-insulator waveguide,"** *J. Opt. Soc. Am. B*, vol. 36, pp. A193-A202, Feb. 2019.

[10] M. Kalantari, A. Karimkhani, and Hamed Saghaei, **"Ultra-Wide Mid-IR Supercontinuum Generation in As_2S_3 Photonic Crystal Fiber by Rods Filling Technique,"** *Optik*, vol. 158, pp. 142-151, Apr. 2018.

[11] A. Ghanbari, A. Kashaninia, A. Sadr, and H. Saghaei, **"Supercontinuum generation with femtosecond optical pulse compression in silicon photonic crystal fbers at 2500 nm,"** *Opt. Quant. Electron.*, vol. 50, 411 (12pp), Oct. 2018.

[12] H. Saghaei, M. E. Heidari, and M. K. M. Farshi, **"Midinfrared supercontinuum generation via As_2Se_3 chalcogenide photonic crystal fibers,"** *Appl. Opt*., vol. 54, pp. 2017-2079, Mar. 2015.

[13] L. V. Hieu, H. V. Thuy, G. Stępniewski, L. C. Trung, V. T. M. Ngoc, R. Kasztelanic, M. Klimczak, J. Pniewski, D. X. Khoa, A. M. Heidt, and R. Buczyński, **"Low pump power coherent supercontinuum generation in heavy metal oxide solid-core photonic crystal fibers infiltrated with carbon tetrachloride covering 930–2500 nm,"** *Opt. Express*, vol. 29, pp. 39586-39600, Nov. 2021.

[14] N. T. Thuy, **"Dispersion optimization in GeO_2-doped silica photonic crystal fibers with circular lattice,"** *Majlesi J. Electrical Engineering*, vol. 17, pp. 59-67, Jun. 2023.

[15] C. V. Lanh, V. T.T M. Ngoc, L. T. B. Tran, D. V. Trong, N. T. H. Phuong, D. M. Trang, L. C. Trung, L. V. Hieu, N. T. Thuy, T. D. Thanh, and H. V. Thuy, **"Broadband supercontinuum generation in cascaded tapered liquid core fiber",** *Opt. Communications*, vol. 527, 129441 (11pp), Mar. 2023.

[16] P. Montméat, T. Enot, M. D. M. Dutra, M. Pellat, and F. Fournel, **"Study of a silicon/glass bonded structure with a UV-curable adhesive for temporary bonding applications,"** *Microelectronic Engineering*, vol. 173, pp. 13-21, Mar. 2017.

[17] T. Baghdasaryan, K. Vanmol, H. Thienpont, F. Berghmans, T. Geernaert, and Jü. V. Erps, **"Design and two-photon direct laser writing of low-loss waveguides, tapers and S-bends,"** *J. Phys. Photonics*, vol. 3, 045001 (16pp), Aug. 2021.

[18] L. T. B. Tran, T. T. C. Oanh, N. T. Thuy, and C. V. Lanh, **"Comparison of chromatic dispersion of circular and hexagonal photonic crystal fibers with chloroform-core,"** *Majlesi J. Electrical Engineering*, vol. 16, pp. 55-61, Sep. 2022.

[19] C. V. Lanh, H. V. Thuy, C. L. Van, K. Borzycki, D. X. Khoa, T. Q. Vu, M. Trippenbach, R. Buczyński, and J. Pniewski, **"Supercontinuum generation in benzene-filled hollow-core fibers",** *Opt. Engineering*, vol. 60, 116109 (13pp), Nov. 2021.

[20] L. V. Hieu, H. V. Thuy, N. T. Hue, C. L. Van, R. Buczyński, and R. Kasztelanic, **"Supercontinuum generation in photonic crystal fibers infiltrated with tetrachloroethylene,"** *Opt. Quant. Electron*., vol. 53, 187 (18pp), Mar. 2021.

[21] Y. Guo, J. Yuan, K. Wang, H. Wang, Y. Cheng, X. Zhou, B. Yan, X. Sang, and C. Yu, **"Generation of supercontinuum and frequency comb in a nitrobenzene-core photonic crystal fiber with all-normal dispersion profile,"** *Opt. Communications*, vol. 481, 126555, Feb. 2021.

[22] C. V. Lanh, L. T. B. Tran, N. T. Thuy, H. T. Duc, D. V. Trong, D. M. Trang, T. N. Hoang, T. D. Thanh, and D. Q. Khoa, **"Comparison of supercontinuum generation spectral intensity in benzene-core PCFs with different types of lattices in the claddings",** *Opt. Quant. Electron.,* vol. 54, 840 (1600), Oct. 2022.

[23] M. T. Islam, M. G. Moctader, K. Ahmed, and S. Chowdhury, **"Benzene Shape Photonic Crystal Fiber Based Plasma Sensor: Design and Analysis,"** *Photonic Sensors*, vol. 8, pp. 263-269, Jun. 2018.

[24] H. T. Duc, N. A. Tu, and N. T. Thuy, **"A New Design of Ultra-flat Dispersion Photonic Crystal Fiber using Benzene Infiltration,"** *VNU J. Sci. Mathematics – Phys.,* vol. 39, pp. 42-52, Mar. 2023.

[25] M. A. Habiba and M. S. Anower, **"Square Porous Core Microstructure Fiberfor Low Loss Terahertz Applications,"** *Opt. Spectrosc.,* vol. 126, pp. 607-613, Jun. 2019.

[26] J. F. Algorri, D. C. Zografopoulos, A. Tapetado, D. Poudereux, and J. M. Sánchez-Pena, **"Infiltrated Photonic Crystal Fibers for Sensing Applications,"** *Sensors (Basel)*, vol. 18, 4263 (32pp), Dec. 2018.

[27] G. Stepniewski, R. Kasztelanic, D. Pysz, R. Stepien, M. Klimczak, and R. Buczynski, **"Temperature sensitivity of chromatic dispersion in nonlinear silica and heavy metal oxide glass photonic crystal fibers,"** *Opt. Mater. Express*, vol. 6, pp. 2689-2703, Aug. 2016.

[28] S. Kedenburg, M. Vieweg, T. Gissibl, and H. Giessen, **"Linear refractive index and absorption measurements of nonlinear optical liquids in the visible and near-infrared spectral region,"** *Opt. Mater. Express,* vol. 2, pp. 1588-1611, Oct. 2012.

[29] Lumerical Solutions, http://www.lumerical.com/tcad-products/mode/

[30] K. Saitoh, M. Koshiba, T. Hasegawa, and E. Sasaoka, **"Chromatic dispersion control in photonic crystal fibers: Application to ultra-flattened dispersion,"** *Opt. Express*, vol. 11, pp. 843-852, Apr. 2003.

[31] J. Wang, Z. D. Chen, C. Peng, J. Li, and S. A. Ponomarenko, **"Development of the Recursive Convolutional CFS-PML for the Wave-Equation-Based Meshless Method,"** *IEEE Transactions on Antennas and Propagation*, vol. 69, pp. 3599-3604, Jun. 2021.

[32] P. Gołębiewski, P. Wiencław, J. Cimek, P. Socha, D. Pysz, A. Filipkowski, G. Stępniewski, O. Czerwińska, I. Kujawa, R. Stępień, R. Kasztelanic, A. Burgs, and R. Buczyński, **"3D soft glass printing of preforms for microstructured optical fibers,"** *Additive Manufacturing*, vol. 79, 103899 (11pp), Jan. 2024.

[33] S. Todoroki, **"Quantitative evaluation of fiber fuse initiation with exposure to arc discharge provided by a fusion splicer,"** *Sci. Rep.,* vol. 6, 25366 (16pp), May. 2016.

[34] Z. Zhu and T. G. Brown, "**Full-vectorial finite-difference analysis of microstructured optical fibers,"** *Opt. Express*, vol. 10, pp. 853-864, Aug. 2002.

[35] X. Chen, J. E. Hurley, J. S. Stone, and M. J. Li, **"Chromatic Dispersion Measurements of Single-Mode Fibers, Polarization-Maintaining Fibers, and Few-Mode Fibers Using a Frequency Domain Method,"** *Photonics*, vol. 10, 215 (12pp), Feb. 2023.

[36] W. K. Al-Azzawi, A. K. J. Al-Nussairi, H. R. Taresh, Z. R. Abdulsada, K. Al-Majdi, H. A. Ali, and J. Zhazira, **"Optimization of Energy Systems in a Distribution Micro grid: An Application of the Particle Swarm Optimization,"** *Majlesi J. Electrical Engineering*, vol. 17, pp. 41-46, Jun. 2023.

[37] S. Katoch, S. S. Chauhan, and V. Kumar, **"A review on genetic algorithm: past, present, and future,"** *Multimed Tools Appl.,* vol. 80, pp. 8091-8126, Feb. 2021.

[38] N. T. Thuy, H. T. Duc, and C. V. Lanh, **"Comparison of supercontinuum spectral widths in CCl_4-core PCF with square and circular lattices in the claddings,"** *Laser Phys*., vol. 33, 055102 (13pp), Mar. 2023.

[39] C. V. Lanh, H. V. Thuy, C. L. Van, K. Borzycki, D. X. Khoa, T. Q. Vu, M. Trippenbach, R. Buczyński, and J. Pniewski, **"Supercontinuum generation in photonic crystal fibers infiltrated with nitrobenzene",** *Laser Phys*,. vol. 30, 035105

(9pp), Feb. 2020.
[40] M. E. Heidari, F. Dehgha, H. Saghaei, F. Koohi-Kamali, and M. K. Moravvej-Farshi, **"Dispersion engineering of photonic crystal fibers by means of fluidic infiltration,"** *J. Modern Opt.,* vol. 59, pp. 1384-1390, Aug. 2012.
[41] R. Raei, M. Ebnali-Heidari, and H. Saghaei, **"Supercontinuum generation in organic liquid-liquid core-cladding photonic crystal fiber in visible and near-infrared regions",** *J. Opt. Society of America B*, vol. 35, pp. 323-330, Jan. 2018.
[42] D. V. Trong and C. V. Lanh, "Supercontinuum generation in $C_6H_5NO_2$-core photonic crystal fibers with various air-hole size," *Modern Phys. Lett. B*, vol. 37, 2350063 (15 pp), May 2023.
[43] C. V. Lanh, A. Anuszkiewicz, A. Ramaniuk, R. Kasztelanic, D. X. Khoa, C. L. Van, M. Trippenbach, and R. Buczyński, **"Supercontinuum generation in photonic crystal fibres with core filled with toluene,"** *J. Opt.,* vol. 19, 125604 (9pp), Nov. 2017.
[44] Z. Mohebi, F. Parandin, F. Shama, and A. Hazeri, **"Highly linear wide band low noise amplifiers: A literature review,"** *Microelectron. J*., vol. 95, 104673 (34pp), Jan. 2020.
[45] L. Caprini, H. Löwen, and R. M. Geilhufe, **"Ultrafast entropy production in pump-probe experiments,"** *Nat. Commun.,* vol. 15, 94 (10pp), Jan. 2024.
[46] C. Wang, T. He, H. Zhou, Z. Zhang, and C. Lee, **"Artificial intelligence enhanced sensors - enabling technologies to next-generation healthcare and biomedical platform,"** *Bioelectron. Med*., vol. 9, 17 (34pp), Aug. 2023.
[47] R. Gayathri ,C. S. S. Sandeep, C. Vijayan, and V. M. Murukeshan, **"Lasing from Micro- and Nano-Scale Photonic Disordered Structures for Biomedical Applications,"** *Nanomaterials*, vol. 13, 2466 (23pp), Aug. 2023.